# V-disparity Based UGV Obstacle Detection in Rough Outdoor Terrain

Yang Cong[1,2], Junjian Peng[1,2], Jing Sun[1,2], Linlin Zhu[1,2], Yandong Tang[1]

**Abstract** This paper presents a fast obstacle detection (OD) system based on stereo vision for Unmanned Ground Vehicle (UGV) navigation in unstructured environment. In order to make the UGV adaptable to more complex terrains, we propose a new estimation method of the Main Ground Disparity (MGD) from the V-disparity images. Then by comparing the disparity of the MGD with local 3D reconstruction, a Coarse-to-Fine method to find and localize obstacles is introduced in the paper. The obstacle detection system is tested practically on our UGV platform in some outdoor unstructured environments. The experimental results validate the efficacy of our system.

**Key words** MGD, V-disparity image,obstacle detection, UGV, outdoor unstructured environment

## 1 Introduction

The ability to detect obstacle autonomously is very crucial to the safety of mobile robots and robot navigation. Therefore, it has received a great deal of attention in recent years. Guilherme et al [1] gave a particular survey about vision technologies for mobile robot navigation in 2002. According to the specific applications environment,the autonomous obstacle detection and navigation technology can be classified into the indoor environment and outdoor environment; and according to the topographical features, it can be classified into the structured environment and unstructured environment. Mobile robot navigation in the indoor and structured environments has achieved great progress and success due to the simplicity of the scenes and the terrains. One of the most prominent pieces of work is the Navlab project[2], in which the UGV autonomously travelled across the American continent from the west coast to the east coast, where the UGV was navigated using neural-network based vision system. On the other hand, the outdoor navigation has broad applications, such as agriculture, military, planet rover,etc. There is still a challengeable problem due to its complex environment and various disturbing factors, which require the UGV to have more powerful perception ability.

In rough outdoor terrain, two main sensors: laser range finder and camera, have been widely adopted for navigation and obstacle detection. Although laser sensors provide refined and easy-to-use information about the surrounding area, they also have some intrinsic limitations, such as one degree of freedom, larger huge, higher energy consumption, etc. On the contrary, vision system has plenty of merits, such as the ability to handle larger amount of data, lower energy consumption, smaller size, higher resolution, etc. Though the vision algorithm is more complex, it is still with broader prospects and our work intends to improve it.

### 1.1 Related work

According to the number of cameras, the vision based OD for outdoor unstructured environment can be classified into Monocular, Binocular and Multi-cameras methods.

**Monocular Vision based methods:** **Optical Flow** was used for robotics obstacle detection in [15], however it could not give an accurate localization of the obstacles. **Appearance** based method [16] applied only appearance or color feature to distinguish the obstacles. Recently, some research on **3D Reconstruction from Single Still Image** were presented to detect obstacle [17,18,19]. These methods intended to recover the absolute depth of the scenarios by features extraction and machine learning, thus, they cannot give the global 3D localization and need strong prior knowledge which were not always available in outdoor conditions. The general problem of monocular vision method is that it cannot get precise global 3D information and is always based on strong prior constraints. As we knew, none of monocular vision systems achieve practical application in rough outdoor terrain.

**Binocular and Multi-cameras Vision based methods:** Most research were mainly based on **Disparity** calculation or **Global 3D Reconstruction**, such as, the pioneer Demo III program [3], Mars Rover vision system [5], the winner of DARPA 2006 [6], OD for high grasses and shadows [7], NASA's stereo vision system by integrated laser sensor [8]. JPL[4] gave particular evaluation on several OD algorithms for seven different typical obstacles based on disparity or global 3D reconstruction methods. In 2005, a novel algorithm, called **V-disparity** image [9,10,11], was designed to detect obstacles by estimating the disparity of the ground plane automatically. There were also Bernd's **Ground Plane Segment** technology[12,13]. In summary, there are two imperfect points about the above methods. One is the flat ground plane assumption, which is not always available in outdoor unstructured environment and hence became a potential limitation. Even the V-disparity image based methods, which had a good result for OD, however their results are also found on the above assumption. The other point of concern is the time consumption. In JPL [8] the flat ground plane assumption is omitted by global 3D reconstruction, but it suffers heavy burden of time consumption.

### 1.2 Our main contributions

In this paper, our original idea is partially motivated by A.Broggi's work[9,10], but, our algorithm is not based on the flat ground plane assumption anymore.

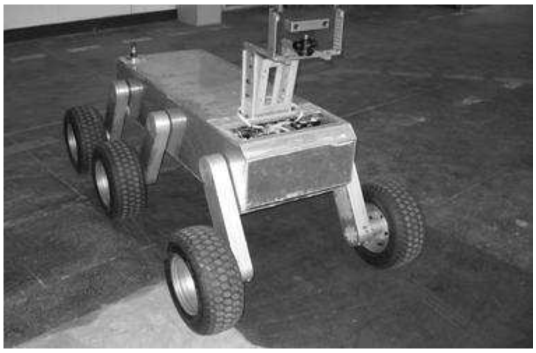

Fig. 1 The UGV: our platform

Received Sept 18, 2008; in revised form April 17, 2009
Supported by National Natural Science Foundation of China (60835004,60871078)
1. State Key Laboratory of Robotics, Shenyang Institute of Automation, Chinese Academy of Sciences, Shenyang 110016, P. R. China 2. Graduate School of the Chinese Academy of Science, Beijing 100038, P. R. China
DOI: 10.3724/SP.J.1004.2008.xxxxx

Our only hypothesis is that most of the region is ground or safe terrain, and we are confident that this, being a very loose constraint, can be easily satisfied. The main contribution of our is described as follows.

I. We introduce a novel method based on the maximum of local energy to extract MGD from the V-disparity image. This has two obvious merits: one is that we can directly detect the obstacles by comparing the disparity with the MGD; the other is that our method can also work even if the gradient of the ground changes discontinuously.

II. We use the Coarse-to-Fine idea to detect obstacles. That is, we find the potential obstacles by comparing the disparity with the ground disparity; then, refine them by a precise 3D local reconstruction to determine whether they belong to final obstacles or not. This makes our algorithm run quickly while keeping the accuracy.

The remainder of this paper is organized as follows. Section 2 describes the hardware system of our UGV. The details of our obstacle detection algorithm are proposed in section 3. The experimental results and the conclusion are presented in section 4 and 5 respectively.

## 2 The system overview

The Unmanned Ground Vehicle (UGV) platform is shown in Figure 1. The UGV is equipped with 6 wheel-and-leg structures that enhance the ability to overcome the obstacles in the complex outdoor terrain. The stereo vision system, with a baseline of 12 cm, is equipped with two color cameras encompassing about 70 degree Field of View (FOV) with a resolution is $640 \times 320$. Therefore, the UGV is nearsighted due to the short baseline. A 1D laser range finder is also fitted out to help the UGV perceive the surrounding. The system is also fitted with an Inertial Measurement Unit (IMU) and a GPS for global localization and navigation. The UGV is equipped with two computers: one is for computer vision processing, including 3D scenario reconstruction and the obstacles detection; the other is for the UGV to control its body, deal with the laser range finder, and global navigation.

## 3 General description

Our obstacle detection algorithm includes the following steps:

I. Preprocessing

II. V-disparity image calculation

III. MGD extraction

IV. Potential obstacle detection

V. Refining obstacle detection and localization

### 3.1 Preprocessing

Both of the left and right images are firstly captured and denoised, and any optical distortions are eliminated to improve the quality of matching. Then the epipolar line constraint is applied to rectify the images. The left and right rectified images are shown in Figure 2 (a) and (b).

### 3.2 V-disparity image calculation

The V-disparity image, the foundation of our OD system, is firstly introduced by [9,10,11], with the intention to reduce the computation burden of disparity image. Rather than following the normal way of generating density disparity image, this method obtains the global disparity information by statistical the consistent phase on the epipolar line. Figure 2 is a synthesized toy demo.

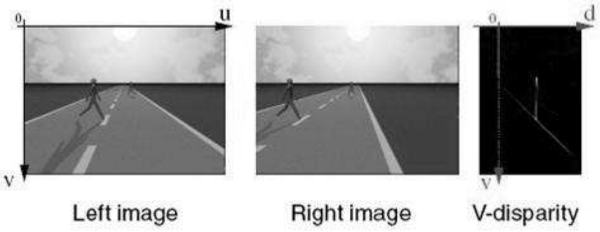


Fig. 2 A V-disparity image example on synthetic images. The frame of reference is plotted. In this case the similarity measures are computed on edges[9].

The V-disparity image can be considered as a 3-D graphical representations of the similarity measures between the left and right image rows (V-coordinate), depending on the disparities (d-coordinate). Brightness is used as the third dimension. The V-disparity image can be understood as the disparity histogram of each row. The higher value of the image means the higher probability of the disparity in the row. In this paper, the V-disparity image is calculated as follows:

A, The Sobel filters is adopted to filter the rectified images, generate and strengthen edge features, as shown in Figure 3(L-2) and (R-2).

B, Then, we get the ternarized image by mapping the obtained values into a ternary domain as equation 1, see Figure 3(L-3) and (R-3).

$$f(x,y) = \begin{cases} -1 & f(x,y) < -\delta \\ 0 & |f(x,y)| \le \delta \\ 1 & f(x,y) > \delta \end{cases} \tag{1}$$

where f(x,y) is the result of filter at point(x,y),$\delta$ is empirically set as 5.

C, The V-disparity image is calculated by equation 2.

$$corr(i,j) = \frac{(N_{match}(i,d))^2}{N_L \cdot N_L} \tag{2}$$

Where $d$ is the disparity value used to compare the two rows, $i$ is the row index, $N_{match}(i,d)$ is the number of phase matching between the left and right rows compared at disparity $d$ at $i$ row, and $N_L$ and $N_R$ are the number of non-block pixels. Figure 3 and Figure 4 (c) show the examples of V-disparity images.

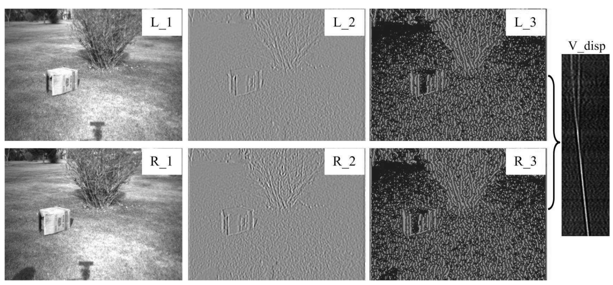


Fig. 3 The flow chart of V-disparity image calculation: the image indexed by 'L-1' is the preprocessed original image, 'L-2' is the result filtered by sobel operator, 'L-3' is the ternarized image; and so do on the same as 'R-1,R-2, R-3', which is the right image. Finally, the image on the right column is the calculated V-disparity image.

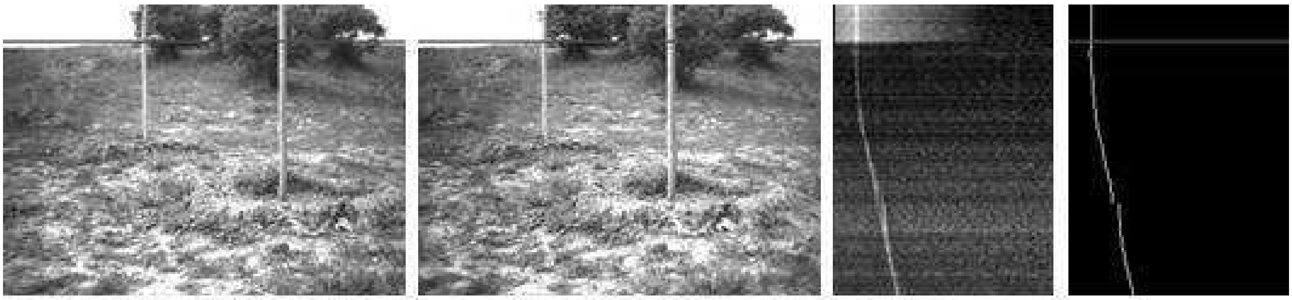


Fig. 4 An example: (a) and (b) are the rectified left and right image respectively, (c) is the V-disparity image, and (d) is the extracted main ground disparity. The main ground disparity is not a straight line because the ground plane is not flat. The region above the red horizon line is far away, it is not need to match and detect obstacles.)

### 3.3 MGD estimation

When most of the terrain is safe for UGV to go across, the disparity value of the pixel with respect to the ground plane will be similar or varying in a minor range in each row of the disparity image. Thus, there will be a high lighting region in each row of the V-disparity image, as shown in Figure 3 or Figure 4. This value is defined as the Main Ground Disparity. From near to far in 3D space (from top to bottom in the image), these values are different and change from high to low. When the ground is flat, the changing is linear, so there is a slopy line in the V-disparity image. In [9,10,11], they used dynamic pitch information and accumulation approach to estimate the possible position of such slopy line. However, the ground plane is not always flat. It may be a cure, and may not always be considered as a straight line. So with this fact, the method [9,10,11] may no always be efficient.

To solve the above problem, we design a novel method to estimate the MGD directly based on maximum local energy. Flat ground plane assumption is no longer the important prerequisite to our method. Our original motivation is that the higher the value is in the V-disparity image, the more the possibility of this disparity exists when matching. Due to the impact of noise and wrong matching, the ground disparity presents a maximum local region in the row of the V-disparity image. The detail of MGD estimation method are as follows:

A, Computing the mean and variance of each row in the V-disparity image by equation 3:

$$\begin{aligned} \mathrm{Mean}(i) &= \frac{1}{N}\sum_{j\in R} I_V(i,j) \\ \mathrm{Var}(i) &= \sqrt{\frac{1}{N}\sum_{j\in R}(I_V(i,j)-\mathrm{Mean}(i))^2} \end{aligned} \tag{3}$$

where $N$ is the width of the V-disparity, i is the row index, j is the column index, $j \in [1 \dots N]$, and $I_V$ denotes the V-disparity image.

B, Setting the dynamic threshold as

$$\mathrm{T_V}(i) = \mathrm{Mean}(i) + 3 \times \mathrm{Var}(i) \tag{4}$$

Where the $T_v(i)$ illustrates the threshold of ith row. If the $I_v$ value of is less than the threshold, it is set as 0; otherwise, we reserve its original value.

C, Now, each line of $I_v$ has been segmented as some isolate regions separated zeros. The region, which is higher than the surroundings may be the MGD, the obstacle, or region caused by noise or wrong matching. The energy of each region is calculated by equation 5.

$$\mathrm{Engery}(k) = \sum_{j\in region(k)} |I_v(i,j)|^2 \tag{5}$$

Where $\mathrm{Engery}(k)$ is the aggregate of the point in the region k, and $\mathrm{Engery}(k)$ is the energy of region k.

D, The region with the maximum local energy value should be the ground. Therefore, the center of this region is the MGD in this row. Another restriction is the MGD value of the topper row will less than or equal to the value of the bottom row. This is easy to understand that the above row indicates the farther region, so the disparity will be less than the near region.

E, Repeating to A to estimate the MGD of each row. Figure 3 and Figure 4 (d) illustrate the results of extracting the main ground disparity

### 3.4 Potential obstacle detection

The MGD has two main functions: reducing the processed areas and detecting potential obstacles.

Let us explain the first function firstly. When parameters of the stereo vision system are fixed, the accuracy of the $3D$ reconstruction is inverse ratio to the distance of the objects; hence from equation 6, we can conclude that $Z$ is inverse ratio to the disparity. That is, the smaller disparity means the farther distance $Z$. Therefore, the smaller the disparity is, the worse the accuracy will be.

$$\begin{cases} \mathrm{Z} = \mathrm{B} \times \mathrm{F}/\triangle \\ \mathrm{X} = \mathrm{Z} \times u/\mathrm{F} = \mathrm{B} \times u/\triangle \\ \mathrm{Y} = \mathrm{Z} \times v/\mathrm{F} = \mathrm{B} \times v/\triangle \end{cases} \tag{6}$$

where X,Y and Z are the 3D point coordinates, B is the width of the baseline, F is the focal length, $\Delta$ is the disparity, u and v are the 2D image pixel coordinates. If we want to get an accurate reconstruction result, we should abandon the pixels with minor disparity, which can reduce the time consumption and increase accuracy. A disparity threshold is preset as 5 to achieve it. If the MGD of some row is less than the threshold, we neglect it. For example, in Figure 4, the MGD of the region above the red line are less than the threshold, they will be too far to be processed anymore.

The second function of MGD is to detect the potential obstacles by comparing the disparity of each pixel with the value of MGD in the same row. The image matching is a precondition to calculate the disparity. Daniel et al[1] present a particular survey about this field in 2003. The matching method can be classified into two types: the local methods and the global methods.

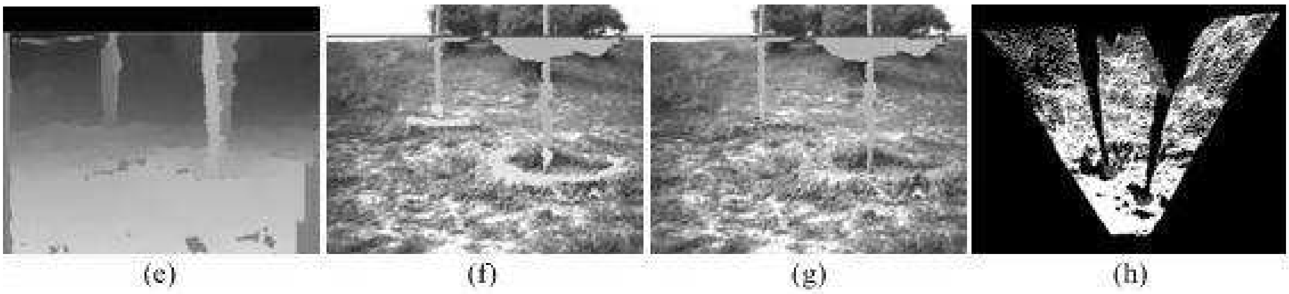


Fig. 5 (e) is the disparity image matched by (a) and (b); (f) is the potential obstacle detection result, both of the yellow and blue regions are potential obstacles; (g) is the refining obstacle detection result, the yellow regions are the false obstacles, so they are eliminated finally; (h) is the bird's eye view maps of the 3D points cloud, and the red points indicate the detected obstacles. )

In this paper, a traditional local method with gray feature, SAD (Sum of Absolute Difference), is chosen to calculate the disparity. Assume a 2D $m \times n$ pattern or block, g(x,y), is to be matched within an image or search area f(x,y) with size $w \times h$, where ($w > n$ and $h > n$). For each pixel location (x,y) in the image, the SAD is calculated as follows:

$$SAD(x,y) = \sum_{l=0}^{n-1}\sum_{k=0}^{m-1} |f(x+k, y+l) - g(k-l)| \quad (7)$$

where $f(k,l)$ and $g(k,l)$ denote the gray level of the two rectified images, $n$ and $m$ are the width and height of the template respectively. The potential obstacle points are extracted on the principle that if the disparity of some point is larger than the main ground disparity of its row, it may be the obstacle point, as shown in equation 8.

$$|\Delta(i,j) - V_\Delta(i)| > Threshold \quad (8)$$

Where $\Delta$ is the disparity, $i$ and $j$ are the row and column coordinates respectively, $V_\Delta(i)$ is the MGD of $i_{Th}$ row, and $Threshold$ is set to 5.

After all of the potential obstacle points have been found, they are clustered into different regions. If the area of some region is relatively less than a threshold (area threshold is preset as 50), it will be a disturbing region (not a potential obstacle region) to be eliminated. Figure 5(f) is the potential obstacle detection result. Both of the yellow regions (false obstacles) and blue regions (true obstacles) are potential obstacles, and the false obstacles will be eliminated in the next section.

### 3.5 Refining obstacle detection and localization

The final obstacles are determined mainly by two criteria: the slope of the local surface is higher than a certain value, and it spans a vertical interval larger than some threshold. In this paper, the maximum relative height and slope of the obstacle are 30 centimeters and 45 degrees respectively, which are determined by UGV platform. The above definitions are related to the world coordinate system. If the UGV changes its attitude, such as pitch angle, the UGV coordinate system also transfers relative to the world coordinate system. Thus there exists a transformation between the world coordinate system and the UGV body coordinate system, as shown in equation 9.

$$\begin{aligned} O_w &= [R|T]O_c \\ R &= \begin{vmatrix} C_\phi C_\theta C_\psi - S_\phi S_\psi & -C_\phi C_\theta C_\psi - S_\phi C_\psi & C_\phi S_\theta \\ S_\Phi C_\Theta C_\Psi + S_\Phi S_\Psi & -S_\Phi C_\Theta C_\Psi + C_\Phi C_\Psi & S_\Phi S_\Theta \\ -S_\Theta S_\Psi & S_\Theta S_\Psi & C_\Theta \end{vmatrix} \\ T &= [x, y, z, 1]^T \end{aligned} \quad (9)$$

Where $[\Phi, \Theta, \psi]^T$ denotes the attitude angle vector, which are the yaw angle, pitch angle and roll angle, T is the position vector of direction $x$, $y$ and $z$, $O_c$ is the centre of the camera coordinate (UGV coordinate system), and $O_w$ is the centre of the world coordinates.

We extract the final obstacle region and calculate some of its parameters, such as the distance, the yaw angle, the width and the length of the obstacle. These parameters can be applied to plan the path, steer the vehicle to make it much safer in the complex outdoor environment. Figure 5(g) is the refined obstacle detection result, and the yellow regions are the false obstacles to be eliminated. Figure 5 (h) is the bird's eye view maps of the 3D points cloud, and the red points indicate the detected obstacles.

## 4 Experimental results

In this section, an evaluation of the obstacle detection algorithm is proposed. The experiments are done under various outdoor unstructured environments with normal obstacles. The obstacles can be classified, by their relative heights to the ground, into two classes: the positive obstacles, including the big stones, high bushes, trunks and even moving targets; and the negative obstacles, mainly deep ditches. In each scene, the UGV is moving along a preset path. The obstacles, around both sides of the path, will be entered into the Field of View (FOV) consecutively.

The performance of our algorithm is evaluated by two factors: the accuracy of detection and the accuracy of localization. The former is for our OD algorithm. In the experiments, the vision system can detect nearly all of the obstacles in the FOV in all of the scenarios, except two bushes with around 30cm relative heights, which the system considered by mistake. Figure 6 and Figure 7 present some obstacle detection results including bushes and tall thin tree trucks, which often exist in the outdoor terrain. Figure 8 and Figure 9 illustrate some other obstacle detection results, including negative obstacles and positive obstacles. From the results, we can conclude that our obstacle detection algorithm is also effective even for deep ditches and moving obstacles.

The accuracy of localization relates to the accuracy of the stereo vision system determined by the width of baseline (The maximum effective distance of our vision system is 10 meters, with $1\%$ errors acceptable).

All the experiments are carried out using a laptop computer with a P4 2.8 GHz processor and 1G Mb of RAM, the average time consumption is up to 200ms on $640 \times 320$ pixels images.

## 5 Conclusion and future work

This paper presents a fast obstacle detection algorithm based on stereo vision for UGV outdoor navigation. Mainly, there are two contributions of this paper: one is that we design a novel method which can extract the main ground disparity from the V-disparity image by maximum local energy. It makes the UGV suitable to more complex terrain. The other is that we use the Coarse-to-Fine idea to detect the obstacle and judge whether the UGV can overcome it. The experiment results have validated the effectiveness of our algorithm. In the future, we plan to improve our obstacle detection algorithm which will be tested under much more complex conditions. The laser sensor data will be fused with the vision information, and the terrain classification approach will be also integrated into our algorithm based on the machine learning method.

## Acknowledgement

Thanks to Claudio Caraffi for giving us some valuable advices about their V-Disparity algorithm, as these are very helpful for our work.

**References**


1 DeSouza G N, Kak A C, Vision for mobile robot navigation: a survey. *IEEE Transactions on Pattern Analysis and Machine Intelligence*, 2002, **24**(2): 237-267

2 D. Pomerleau, *Neural network vision for robot driving*. The Handbook of Brain Theory and Neural Networks, M. Arbib, ed. MIT Press,1995.

3 Bellutta P, Manduchi R, Matthies L, Owens K, Rankin A. Terrain perception for DEMO III. In:Proceedings of IEEE Conference Intelligent Vehicles Symposium. Dearborn(MI),USA: IEEE 2000. 3-5

4 Matthies L, Maimone M, Johnson A, Cheng Y, Willson R, Villalpando C, et al. Computer Vision on Mars. *International Journal of Computer Vision*, **2007**, 75(1): 67-92.

5 Rankin A, Huertas A, Matthies L, Evaluation of stereo vision obstacle detection algorithms for off-road autonomous navigation. AUVSI Symp. on Unmanned Systems, 2005

6 Thrun S, Montemerlo M, Dahlkamp H, Stavens D, Aron A, Diebel J. et al Stanley, the robot that won the DARPA Grand Challenge. *Journal of Field Robotics*, **2007**,23(9): 661-692.

7 Konolige K, Agrawal M, Bolles R C, Cowan C, Fischler M, Gerkey B. Outdoor Mapping and Navigation using Stereo Vision. In Proc. of Intl. Symp. on Experimental Robotics (ISER) Rio de Janeiro, Brazil, 2006

8 Manduchi R, Castano A, Talukder A, Matthies L. Obstacle detection and terrain classification for autonomous off-Road navigation. *Autonomous Robots*, **2005**,18(1): 81-102

9 Broggi A, Caraffi C, Fedriga R I, Grisleri P. Obstacle detection with stereo vision for off-Road vehicle navigation. In:Proceedings of IEEE Computer Conference on Computer Vision and Pattern Recognition. San Diego,USA: IEEE, 2005.

10 Broggi A, Caraffi C, Porta P P , Zani P. The Single Frame Stereo Vision System for Reliable Obstacle Detection used during the 2005 DARPA Grand Challenge on TerraMax, In: Proceedings of IEEE Conference on Intelligent Transportation Systems. Toronto, Canada: 2006. 745-752.

11 Caraffi C, Cattani S, Grisleri P. Off-Road path and obstacle detection using decision networks and stereo vision, *IEEE Transactions on Intelligent Transportation Systems*, **2007**,8(4):607-618,

12 Schafer B H. Terrain Negotiation in Rough Outdoor Environment, Technical Report, Department of informatics Kaiserslautern University of Technology, 2005

13 Bernd Helge Schafer. Security Aspects of Motion Execution in Outdoor Terrain[Diploma Thesis], Robotics Laboratory Department of Computer and Information Science Kaiserslautern University of Technology, 2005

14 Scharstein D, Szeliski R. A Taxonomy and Evaluation of Dense Two-Frame Stereo Correspondence Algorithms. *International Journal of Computer Vision*, **2002**,47(1-3): 7-42

15 Coombs D, Herman M, Hong T ,Nashman M. Real-time obstacle avoidance using central flow divergence and peripheral flow, *Robotics and Automation*, **1998**,14(1):49-59.

16 I. Ulrich, and I. Nourbakhsh. Appearance-based obstacle detection with monocular color vision, In: Proceedings of AAAI Conference,2000,866-871.

17 Saxena A, Chung S H, Ng A Y. 3-D depth reconstruction from a single still image, *International Journal of Computer Vision*, **2008**,76(1):53-69.

18 Klarquist W N , Geisler W S. Maximum likelihood depth from defocus for active vision, In : Proceedings of the IEEE Conference on interlligent Robots and Systems, 1995,374-379,

19 Rajagopalan A N, et al. Depth estimation and image restoration using defocused stereo pairs , *IEEE Transactions on Pattern Analysis and Machine Intelligence*, **2004** 26(11): 1521-1525,.


**Yang Cong** Ph. D. candidate at the State Key Laboratory of Robotics, Shenyang Institute of Automation, Chinese Academy of Sciences. He received his bachelor degree from Northeast University in 2004. His research interest covers computer vision, pattern recognition, and robotics.
E-mail: congyang81@gmail.com

**Jun-Jian Peng** Master candidate In State Key Laboratory of Robotics in Shenyang Institute of Automation(SIA), Chinese Academy of Sciences(CAS). His research interest covers robot navigation and intelligent video surveillance.
E-mail: junjianp@gmail.com

**Jing Sun** Jing Sun graduated from Northeast University, P.R. China, in 2003, she received the M.S. degree from Dalian Maritime University in 2006. She is currently a PhD student at State Key laboratory of Robotics Shenyang Institute of Automation, Chinese Academy of Sciences. Her research interests include Retinex, and image processing.
E-mail:sunjing@sia.cn

**Linlin Zhu** Ph.D. candidate at Shenyang Institute of Automation, Chinese Academy of Sciences. She received B.S. and M.S. degrees in the department of automatic, Northeast University, P.R. China, in 2004 and 2007. Her research interests include pattern recognition, level set methods and tracking object in sequence frames.
E-mail: zhulinlin@sia.cn

**Yandong Tang** (The Corresponding author of this paper) received B.S. and M.S. degrees in the Department of Mathematics, Shandong University in 1984 and 1987 respectively. In 2002, he received his Ph.D. in Applied Mathematics from the University of Bremen, Germany. Currently he is a Professor in State Key laboratory of Robotics, Shenyang Institute of Automation, Chinese Academy of Sciences. His research interests include image processing, computer vision and numerical computation.
E-mail: ytang@sia.cn

(a) (b) (c)

Fig. 6 Detecting thin trucks. (a) the original right image, (b) the obstacle detection result (the obstacle is indicated by light blue), (c) the bird's eye view maps (the red points are the obstacles and the white points are the background).

(a) (b) (c)

Fig. 7 Another example of detecting bushes and thin trucks in different scenario. (a) the original right image, (b) the obstacle detection result (the obstacle is indicated by light blue), (c) the bird's eye view maps (the red points are the obstacles and the white points are the background).

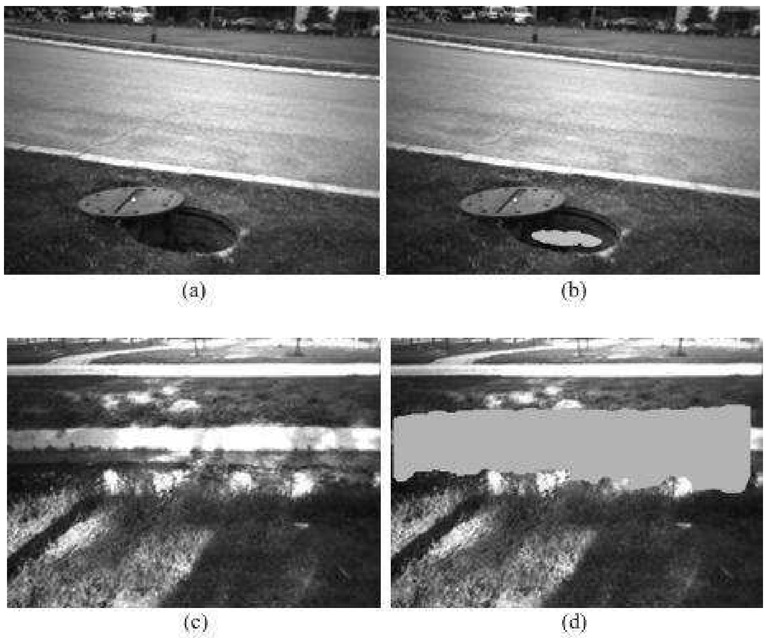


Fig. 8 The negative obstacle (water well) and its detection result in different scenarios (the obstacle is indicated by light blue)

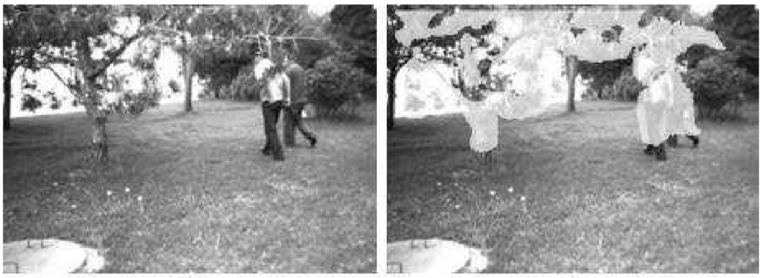

(a) (b)

Fig. 9 The positive obstacles (tree, bushes and moving persons) and their detection results (the obstacles are indicated by light blue)